AIAA 81-0615R

Dynamic Stability of a Rotor Blade Using Finite Element Analysis

Nithiam Ti Sivaneri* and Inderjit Chopra†
Stanford University, Stanford, Calif.

The aeroelastic stability of flap bending, lead-lag bending, and torsion of a helicopter rotor blade in hover is examined using a finite element formulation based on Hamilton's principle. Quasisteady two-dimensional airfoil theory is used to evaluate the aerodynamic loads. The rotor blade is discretized into beam elements, each with ten nodal degrees of freedom. The resulting nonlinear equations of motion are solved for steady-state blade deflections through an iterative procedure. The flutter solution is calculated assuming blade motion to be a small perturbation about the steady solution. The normal mode method based on the coupled rotating natural modes about the steady deflections is used to reduce the number of equations in the flutter eigenanalysis. Numerical results are presented for hingeless and articulated rotor blade configurations.

Nomenclature

a = lift curve slope
A = blade cross section area
B_1, B_2 = blade cross section integrals
c = blade chord
C_D = blade-section drag coefficient
C_{D0} = blade-section profile drag coefficient
C_L = blade-section lift coefficient
$C_{M_{ac}}$ = blade-section pitching moment coefficient
C_T = rotor thrust coefficient, $T/\pi\rho\Omega^2R^4$
C_1, C_2 = blade cross section integrals
e_a = tension center offset from elastic axis, positive forward
e_d = aerodynamic center offset from elastic axis, positive aft
e_g = center of mass offset from elastic axis, positive forward
E = Young's modulus
F = centrifugal force
GJ = blade elastic torsion stiffness
I_b = blade mass moment of inertia about flap axis at the root
I_y, I_z = blade cross section moments of inertia in the flap and lead-lag directions, respectively
k_A = polar radius of gyration of blade cross section, $\sqrt{(I_y+I_z)/A}$
k_m = mass radius of gyration of blade cross section, $\sqrt{(k_{m1}^2+k_{m2}^2)}$
k_{m1}, k_{m2} = principal mass radii of gyration of blade cross section
l_i = length of ith element
L_u, L_v, L_w = aerodynamic forces per unit length in u, v, w directions, respectively
m = mass per unit length of blade
m_0 = reference mass per unit length
M = Mach number
M_ϕ = aerodynamic moment per unit length about elastic axis
n = number of elements
$\{q\}$ = vector of global degrees of freedom
R = rotor radius
t = time
u, v, w = elastic displacements in the x, y, z directions, respectively
U_p, U_T = blade cross section air velocity components in the negative η and ζ directions, respectively
v_i = induced inflow
V = blade section resultant air velocity
x, y, z = undeformed blade coordinates
x_i = local axial coordinate of the ith element
α = section angle of attack
β_p = blade precone angle
γ = Lock number, $\rho acR^4/I_b$
$\delta T, \delta U$ = variation of kinetic and strain energies, respectively
δW = virtual work done due to aerodynamic loads
ϵ = nondimensional order of magnitude parameter
θ = blade pretwist
λ_i = rotor inflow ratio, $v_i/\Omega R$
ξ, η, ζ = deformed blade coordinates
σ = solidity ratio
ϕ = elastic twist about elastic axis
$\hat{\phi}$ = geometric twist about deflected elastic axis
ψ = dimensionless time, Ωt
$\omega_v, \omega_w, \omega_\phi$ = fundamental coupled rotating lead-lag, flap, torsion natural frequencies, respectively
Ω = rotor blade angular velocity
$(\,)'$ = $\partial(\,)/\partial x$
$(\dot{\ })$ = $\partial(\,)/\partial\psi[\partial(\,)/\partial t$ in Eqs. (5), (13), and (15)]

Presented as Paper 81-0615 at the AIAA Dynamics Specialists Conference, Atlanta, Ga., April 9-10, 1981; submitted April 24, 1981; revision received Oct. 19, 1981.

*Research Assistant, NASA/Stanford Joint Institute for Aeronautics and Acoustics. Member AIAA.

†Senior Research Associate, NASA/Stanford Joint Institute for Aeronautics and Acoustics; presently, Associate Professor, University of Maryland, College Park, Md. Member AIAA.

Introduction

HELICOPTER dynamics is a complex problem involving nonlinear structural, inertial, and aerodynamic forces. For the design and analysis of rotors, it is necessary to solve for the trim deflections of blades in hover and forward flight, and to calculate the aeroelastic stability. For efficient blade designs, there is an increasing tendency toward nonuniformity in structural and aerodynamic properties. The blade root geometry is complex and also there is redundancy in load paths, particularly with bearingless rotors.

The simplest form of rotor blade representation is the rigid blade model with spring restrained hinges.[1] For this model, the trim solution is generally obtained from nonlinear flap-lag equations; and the flutter stability is calculated assuming

linear perturbation motion about the trim deflection. This type of solution is satisfactory for very simple blade configurations (for example, articulated). A better representation of the rotor blade is to treat it as an elastic beam. The governing set of coupled equations of an elastic blade has been derived by Houbolt and Brooks.[2] Hodges et al.[3,4] have modified these equations in an attempt to consistently include the nonlinear structural and inertial terms for moderately large deflections. The common approach for calculating the trim deflections, as well as the aeroelastic stability, is the modal method (for example, Galerkin) using uncoupled nonrotating beam modes[5] or coupled rotating natural blade modes.[5,6] In general, it is assumed that the trim deflections are large and the flutter motion is a small perturbation about the trim solution. The solution procedure gets fairly involved for forward flight because of the presence of periodic terms.

It is difficult to apply modal methods to nonuniform blades and blades with complex root geometries. Also, the formulation has to be modified considerably when a different rotor configuration is considered. The finite element method, which has been extensively used in linear structural analysis,[7] has a great potential for solving complex blade dynamics problems. The analysis consists of discretizing the blade into small beam elements and using energy principles or the method of weighted residuals to obtain the forces (inertial, elastic, etc.) over each element. The global equations of motion are obtained by the assembly of the elements. Nonuniformities in blade properties can be accommodated easily. Special elements can be used near the root to take care of complex root geometries and multiple load paths. The finite element method is very flexible and the formulation can be easily adapted to different rotor blade configurations.

The finite element method has been applied for the determination of free vibration characteristics of rotating beams (one dimensional) by many authors.[8-11] It is common practice to use simple beam elements satisfying the continuity of the displacement and slope between elements. Refined elements with internal nodes can also be used. One can attain a desired accuracy by using either simple or refined beam elements, but, if simple elements are used, a greater number of them may be necessary. However, the assembly of simple elements results in narrowly banded matrices; the assembled matrices for refined elements are more populated.

Murty and Raman[12] have applied the finite element method for computing the nonlinear response of a rotating beam under prescribed forces. Yasue[13] has discretized a flap-lag-torsion blade into finite elements to obtain the natural modes and applied the modal method to calculate the trim solution and response of the blade under gust loading. Friedmann and Straub[14,15] have used a Galerkin-type finite element method to find the natural vibration characteristics of a flap-lag blade and computed the trim solution, stability and response of the blade in hover, as well as forward flight. References 13-15 use a modal approach in obtaining the trim solution.

In the present paper, the finite element formulation is used to investigate the stability of flap bending, lead-lag bending, and torsion of a rotor blade in hover. The blade is discretized into simple beam elements, each with ten nodal degrees of freedom. The element forces are obtained applying Hamilton's principle; and the assembly of the elements yields the equations of motion in terms of the nodal degrees of freedom. The nonlinear trim (steady-state) solution is calculated from these equations through an iterative procedure. Then, the coupled rotating free vibration characteristics of the blade about the steady deflections are obtained. The normal mode method based on these natural modes is used to solve the linearized flutter equations.

This is the first attempt to solve the nonlinear trim equations of a flap-lag-torsion blade using the finite element analysis directly. This approach involves very few algebraic manipulations and is much simpler than the modal methods. Furthermore, this procedure enables the natural rotating modes to be calculated about the steady deflected position of the blade.

The formulation is made for a nonuniform blade with pretwist, precone, and having chordwise offsets of the center of mass, aerodynamic center, and tension center from the elastic axis. Quasisteady strip theory is used to obtain the aerodynamic loads. Noncirculatory airloads are also included. Numerical results are presented for a simple example of a blade with uniform properties; the hingeless and articulated rotor blade configurations are considered.

Formulation

The rotor blade is treated as an elastic beam rotating with constant angular velocity Ω. The rectangular coordinate system x, y, z is attached to the undeformed blade which is at a precone angle of β_p (Fig. 1). The origin is at the root of the blade, the x axis coincides with the elastic axis, and the y axis is in the plane of rotation pointed toward the leading edge. The deformed position of the blade is defined by the following sequence. A point P on the undeformed elastic axis undergoes displacements u, v, w in the x, y, z directions, respectively, and occupies the position P′ on the deformed elastic axis. Then the blade cross section containing P′ undergoes a rotation θ_1 about the deformed elastic axis. The orientation of the deformed-beam cross section with respect to the undeformed-beam cross section is described by a sequence of three rotations. This analysis uses the lag-flap-pitch sequence of rotations defined in Ref. 4. The third angle in the sequence θ_1 is written as

$$\theta_1 = \theta + \hat{\phi} \qquad \hat{\phi} = \phi - \int_0^x v'' w' \, dx \tag{1}$$

where θ is the pretwist, $\hat{\phi}$ the geometric twist, and ϕ the elastic twist due to torsion. The orthogonal coordinate system ξ, η, ζ is attached to the deformed blade such that the ξ axis is tangential to the deflected elastic axis and the η and ζ axes are the principal axes of the cross section. The transformation between the two coordinate systems is given as

$$\begin{Bmatrix} i_\xi \\ i_\eta \\ i_\zeta \end{Bmatrix} = [T] \begin{Bmatrix} i_x \\ i_y \\ i_z \end{Bmatrix} \tag{2}$$

The transformation matrix $[T]$ for the lag-flap-pitch sequence is defined in Ref. 4. For moderate rotations such that v'^2, w'^2, $\phi^2 \ll 1$, the matrix $[T]$ is approximated in Ref. 3. This approximate matrix is used in obtaining the equations of motion in the present analysis. The equations of motion are obtained using Hamilton's principle

$$\int_{t_1}^{t_2} (\delta U - \delta T - \delta W) \, dt = 0 \tag{3}$$

where δU, δT, and δW are, respectively, the variation of strain energy, the variation of kinetic energy, and the virtual work

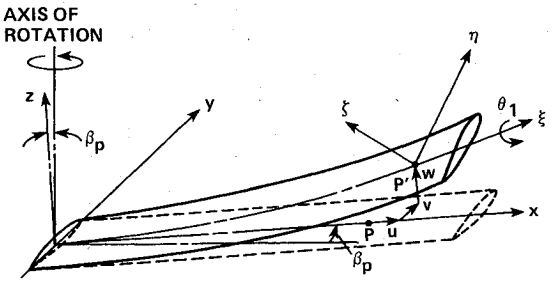

Fig. 1 Blade coordinate systems and deflections.

done. Hodges and Dowell[3] have given expressions for δU and δT. The expression for δW is

$$\delta W = \int_0^R (L_u \delta u + L_v \delta v + L_w \delta w + M_\phi \delta\psi)\,dx \tag{4}$$

where L_u, L_v, L_w, and M_ϕ are the external loads distributed along the length of the blade in the axial, lag, flap, and torsion directions, respectively, and the virtual rotation $\delta\psi$ is[4]

$$\delta\psi \simeq \delta\hat{\phi} + w'\delta v'$$

Equation (3) would result in four equations of motion representing δu, δv, δw, and $\delta\hat{\phi}$, respectively. The δu equation is

$$F = \int_x^R m(\Omega^2 x + 2\Omega\dot{v})\,dx \tag{5}$$

The centrifugal force F can be also expressed as

$$F = EA[u' + \tfrac{1}{2}v'^2 + \tfrac{1}{2}w'^2 + k_A^2\theta'\phi' - e_a(v''\cos\theta_1 + w''\sin\theta_1)] \tag{6}$$

The axial displacement u is eliminated from the virtual energy expressions δU, δT, and δW using Eqs. (5) and (6). Then $\delta U, \delta T$, and δW are nondimensionalized by dividing the expressions by $m_0\Omega^2R^3$, where m_0 is a reference mass per unit length (for example, the value of m at $0.5R$). This is done to see the relative order of magnitude of each term. The nondimensional displacements v/R, w/R, ϕ are assumed to be of order ϵ where ϵ is a small nondimensional parameter such that $\epsilon^2 \ll 1$. The other nondimensional quantities and their assumed orders of magnitude are given in the Appendix. The lowest-order (i.e., first-order) terms in δU and δT are of order ϵ^2. The terms of order ϵ^2 and ϵ^3 are retained while neglecting all terms of order ϵ^4 (i.e., third order) and higher, excepting some linear third-order terms which are important for the torsion equation. The following simplified nondimensional expressions for δU and δT result.

$$\begin{aligned}
\delta U/(m_0\Omega^2R^3) = \int_0^1 \Big\{ & F(v'\delta v' + w'\delta w') + GJ(\hat{\phi}'\delta\hat{\phi}' + \hat{\phi}'w'\delta v'' + \hat{\phi}'v''\delta w' + v''w'\delta\hat{\phi}') + [Fk_A^2(\theta' + \underline{\hat{\phi}'}) - \underline{\underline{EAk_A^4\theta'^2\phi'}} \\
& + \underline{\underline{EAe_ak_A^2\theta'(v''\cos\theta_1 + w''\sin\theta_1)}} + EB_1\theta'^2\hat{\phi}' - EB_2\theta'(v''\cos\theta_1 + w''\sin\theta_1)]\delta\hat{\phi}' + [\underline{\underline{EC_1\hat{\phi}''}} + EC_2(w''\cos\theta_1 - v''\sin\theta_1)]\delta\hat{\phi}'' \\
& + [-Fe_a\cos\theta_1 + \{EI_z\cos^2(\theta+\underline{\hat{\phi}}) + EI_y\sin^2(\theta+\underline{\hat{\phi}})\}v'' + \tfrac{1}{2}(EI_z - EI_y)w''\sin 2\theta_1 - EAe_a^2(v''\cos^2\theta_1 + \tfrac{1}{2}w''\sin 2\theta_1) \\
& + (EAe_ak_A^2 - EB_2)\theta'\hat{\phi}'\cos\theta_1 - EC_2\hat{\phi}''\sin\theta_1]\delta v'' + [-Fe_a\sin\theta_1 + \{EI_z\sin^2(\theta+\underline{\hat{\phi}}) + EI_y\cos^2(\theta+\underline{\hat{\phi}})\}w'' \\
& + \tfrac{1}{2}(EI_z - EI_y)v''\sin 2\theta_1 - EAe_a^2(w''\sin^2\theta_1 + \tfrac{1}{2}v''\sin 2\theta_1) + (EAe_ak_A^2 - EB_2)\theta'\hat{\phi}'\sin\theta_1 + EC_2\hat{\phi}''\cos\theta_1]\delta w'' \\
& + [Fe_a(v''\sin\theta_1 - w''\cos\theta_1) + \underline{(EI_z - EI_y)\{\tfrac{1}{2}(w''^2 - v''^2)\sin 2\theta_1 + v''w''\cos 2\theta_1\}}]\delta\hat{\phi}\Big\}dx
\end{aligned} \tag{7}$$

$$\begin{aligned}
\frac{\delta T}{(m_0\Omega^2R^3)} = \int_0^1 m\Big\{ & [v + e_g\cos\theta_1 + 2\beta_p\dot{w} + 2\int_0^x (\dot{v}v' + \dot{w}w')\,dx + 2e_g(\dot{v}'\cos\theta_1 + \dot{w}'\sin\theta_1) - \ddot{v} + e_g\ddot{\hat{\phi}}\sin\theta_1]\delta v \\
& - [\beta_p(x + 2\dot{v}) + \ddot{w} + e_g\ddot{\hat{\phi}}\cos\theta_1]\delta w - [k_m^2\ddot{\hat{\phi}} + \tfrac{1}{2}(k_{m2}^2 - k_{m1}^2)\sin 2\theta_1 + e_gx(w'\cos\theta_1 - v'\sin\theta_1) + e_g\dot{v}\sin\theta_1 + e_g\beta_px\cos\theta_1 \\
& - e_g(\ddot{v}\sin\theta_1 - \ddot{w}\cos\theta_1)]\delta\hat{\phi} - e_g(x\cos\theta_1 + 2\dot{v}\cos\theta_1)\delta v' - e_g(x\sin\theta_1 + 2\dot{v}\sin\theta_1)\delta w'\Big\}dx
\end{aligned} \tag{8}$$

and

$$\frac{\delta W}{(m_0\Omega^2R^3)} = \int_0^1 (L_v\delta v + L_w\delta w + M_\phi\delta\psi)\,dx \tag{9}$$

The singly underlined terms are nonlinear terms and the doubly underlined terms are third-order (ϵ^4) linear torsion terms. Since δU, δT, and δW are independent of the time derivatives of δu, δv, δw, and $\delta\hat{\phi}$, Eq. (3) can be written as

$$\Delta = \delta U - \delta T - \delta W = 0 \tag{10}$$

Aerodynamic Loads

The aerodynamic loads in hover, distributed along the length of the blade, are obtained using a quasisteady two-dimensional airfoil theory. Forces of noncirculatory origin are also included. The induced velocity is assumed to be uniform and steady.

The circulatory forces $\bar{L}_{vc}$, $\bar{L}_{wc}$, and $M_{\phi c}$ in the η, ζ, and ϕ directions, respectively, can be written as (Fig.2)

$$\bar{L}_{vc} = L\sin\alpha - D\cos\alpha \qquad \bar{L}_{wc} = -L\cos\alpha - D\sin\alpha \qquad M_{\phi c} = M_{ac} - L_{wc}e_d \tag{11}$$

where L, D, and M_{ac} are the lift, drag, and pitching moment (about the aerodynamic center) per unit length, α the angle of attack, and e_d the aerodynamic center offset from the elastic axis. The expressions for L, D, and M_{ac} are

$$L=C_L(\alpha,M)\,\tfrac{1}{2}\rho V^2 c \qquad D=C_D(\alpha,M)\,\tfrac{1}{2}\rho V^2 c \qquad M_{ac}=C_{M_{ac}}(M)\,\tfrac{1}{2}\rho V^2 c^2 \tag{12}$$

with

$$V^2=U_T^2+U_p^2 \quad \text{and} \quad \tan\alpha=U_p/U_T$$

The expressions for U_T and U_p are obtained by considering the relative velocity of the blade with respect to the fluid at the three-quarter-chord point of the cross section.

$$U_T=\Omega x\left[\left(1-\frac{v'^2}{2}\right)\cos\theta_1-v'w'\sin\theta_1\right]+\cos\theta_1[\dot v-\hat\phi\eta_r\sin\theta_1+\Omega(u-v'\eta_r\cos\theta_1-w'\eta_r\sin\theta_1)-\Omega\beta_p(w+\eta_r\sin\theta_1)]$$
$$+\sin\theta_1[\dot w+\hat\phi\eta_r\cos\theta_1+\Omega\beta_p(v+\eta_r\cos\theta_1)+v_i]+(v'\cos\theta_1+w'\sin\theta_1)\Omega(v+\eta_r\cos\theta_1) \tag{13a}$$

$$U_p=-\Omega x\left[\left(1-\frac{v'^2}{2}\right)\sin\theta_1+v'w'\cos\theta_1\right]-\sin\theta_1[\dot v-\hat\phi\eta_r\sin\theta_1+\Omega(u-v'\eta_r\cos\theta_1-w'\eta_r\sin\theta_1)-\Omega\beta_p(w+\eta_r\sin\theta_1)]$$
$$+\cos\theta_1[\dot w+\hat\phi\eta_r\cos\theta_1+\Omega\beta_p(v+\eta_r\cos\theta_1)+v_i]-(v'\sin\theta_1-w'\cos\theta_1)\Omega(v+\eta_r\cos\theta_1) \tag{13b}$$

where η_r is the η coordinate of the three-quarter-chord point and v_i the induced velocity.

Substituting Eqs. (12) in Eqs. (11) yields

$$\bar L_{vc}=\tfrac{1}{2}\rho c(C_L U_p V-C_D U_T V) \qquad \bar L_{wc}=-\tfrac{1}{2}\rho c(C_L U_T V+C_D U_p V) \qquad M_{\phi c}=\tfrac{1}{2}\rho c^2 C_{M_{ac}} V^2-e_d\bar L_{wc} \tag{14}$$

The circulatory forces L_{vc} and L_{wc} in the y and z directions are obtained from $\bar L_{vc}$ and $\bar L_{wc}$ using the transformation matrix $[T]$. The noncirculatory components of force are obtained from unsteady thin airfoil theory.

$$L_{wnc}=\tfrac{1}{4}\pi\rho c^2[-\ddot w+\Omega x\dot\phi+(\tfrac{1}{4}c+e_d)\ddot\phi]$$
$$M_{\phi nc}=\tfrac{1}{4}\pi\rho c^2[(\tfrac{1}{4}c+e_d)\ddot w-(\tfrac{1}{2}c+e_d)\Omega x\dot\phi] \tag{15}$$

The induced velocity is obtained from the momentum theory and the pitch of the blade is obtained by combining the momentum and the blade element theories.

$$\lambda_i=k_h\sqrt{(C_T/2)}, \quad \theta_{0.75R}=6C_T/\sigma a+1.5\lambda_i \tag{16}$$

where λ_i is the nondimensional induced velocity $(v_i/\Omega R)$, k_h an empirical factor, C_T the thrust coefficient, σ the solidity ratio, and $\theta_{0.75R}$ the blade pitch at three-quarter span. The expressions for the complete aerodynamic forces in the lead-lag, flap, and torsion directions are

$$L_v=L_{vc} \qquad L_w=L_{wc}+L_{wnc} \qquad M_\phi=M_{\phi c}+M_{\phi nc} \tag{17}$$

In the derivation of these forces, nonlinear rate product terms, such as $\dot v^2$, $\dot w^2$, $\dot v\dot w$ are neglected (quasilinearization). Equations (17) are nondimensionalized by dividing L_v, L_w by $m_0\Omega^2R^2$ and M_ϕ by $m_0\Omega^2R^3$, and terms of order ϵ^3 and higher are neglected.

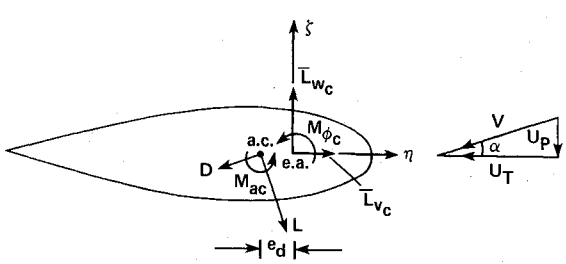

Fig. 2 Deformed blade section aerodynamics.

Finite Element Discretization

The finite element analysis is used to discretize the spatial dependence of the equations of motion. The blade is divided into a number of beam elements. Every element consists of two nodes, denoted by node-1 and node-2 (Fig. 3), with five degrees of freedom namely v, v', w, w', and $\hat\phi$ at each node. The reason for choosing $\hat\phi$ over ϕ as the torsional degree of freedom is as follows. The aerodynamic loads depend explicitly on $\hat\phi$. If ϕ is chosen as the torsional degree of freedom, then the presence of the integral term $\int_0^x v''w'dx$ [Eq. (1)] makes the global matrices nonbanded because of the coupling of the degrees of freedom of one element with that of the other elements. The choice of $\hat\phi$ eliminates this integral and thus preserves the banded structure of the global matrices.

Hamilton's principle, Eq. (10), is discretized as

$$\Delta=\sum_{i=1}^{n}\Delta_i=0 \tag{18}$$

and

$$\Delta_i=\delta U_i-\delta T_i-\delta W_i \tag{19}$$

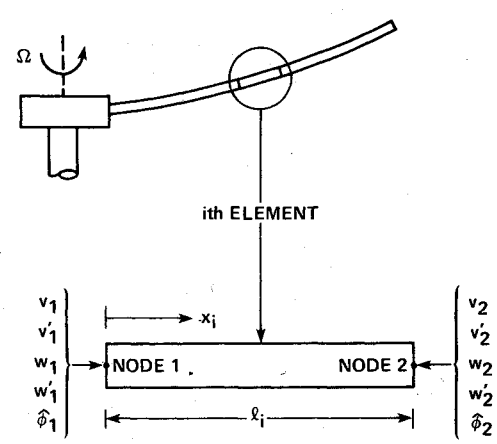

Fig. 3 A finite element showing nodal degrees of freedom.

where δU_i, δT_i, and δW_i are, respectively, the strain energy, kinetic energy, and the virtual work contributions of the ith element. The distribution of the deflections v, w, $\hat{\phi}$ over an element is represented in terms of the nodal displacements using shape functions. For the ith element (Fig. 3),

$$\begin{Bmatrix} v \\ w \\ \hat{\phi} \end{Bmatrix} = [H]\ \{q_i\} \tag{20}$$

where the shape function matrix $[H]$ is

$$[H] = \begin{bmatrix} H_1 & H_2 & H_3 & H_4 & 0 & 0 & 0 & 0 & 0 & 0 \\ 0 & 0 & 0 & 0 & H_1 & H_2 & H_3 & H_4 & 0 & 0 \\ 0 & 0 & 0 & 0 & 0 & 0 & 0 & 0 & H_{\phi_1} & H_{\phi_2} \end{bmatrix} \tag{21}$$

and the vector of element degrees of freedom $\{q_i\}$ is defined as

$$\{q_i\}^D = \lfloor v_1\ v_1'\ v_2\ v_2'\ w_1\ w_1'\ w_2\ w_2'\ \hat{\phi}_1\ \hat{\phi}_2 \rfloor \tag{22}$$

The nodal degrees of freedom at node-1 of the element are v_1, v_1', w_1, w_1', ϕ_1 and those at node-2 are v_2, v_2', w_2, w_2', $\hat{\phi}_2$. The shape functions in Eq. (21) are the Hermite polynomials defined as

$$\begin{aligned} H_1(x_i) &= 2(x_i/l_i)^3 - 3(x_i/l_i)^2 + 1 \\ H_2(x_i) &= l_i[(x_i/l_i)^3 - 2(x_i/l_i)^2 + x_i/l_i] \\ H_3(x_i) &= -2(x_i/l_i)^3 + 3(x_i/l_i)^2 \\ H_4(x_i) &= l_i[(x_i/l_i)^3 - (x_i/l_i)^2] \\ H_{\phi_1}(x_i) &= 1 - x_i/l_i \\ H_{\phi_2}(x_i) &= x_i/l_i \end{aligned} \tag{23}$$

where l_i is the length of the ith element and x_i is the local axial coordinate for the ith element, measured from the left end of the element (Fig. 3). Similar to Eq. (20), the distribution of the virtual displacements δv, δw, and $\delta\hat{\phi}$ over the ith element is assumed to be

$$\begin{Bmatrix} \delta v \\ \delta w \\ \delta\hat{\phi} \end{Bmatrix} = [H]\ \{\delta q_i\} \tag{24}$$

The substitution of Eqs. (20) and (24) in Eq. (19) results in

$$\Delta_i = f(\ddot{q}_i,\ \dot{q}_i,\ q_i,\ \delta q_i)$$

which is nonlinear in q_i. This function can be conveniently written as

$$\begin{aligned} \Delta_i = {} & \{\delta q_i\}^T[M_i(q_i)]\{\ddot{q}_i\} + \{\delta q_i\}^T[C_i(q_i)]\{\dot{q}_i\} \\ & + \{\delta q_i\}^T[K_i(q_i)]\{q_i\} - \{\delta q_i\}^T\{Q_i\} \end{aligned} \tag{25}$$

where $[M_i(q_i)]$, $[C_i(q_i)]$, and $[K_i(q_i)]$ represent the element inertia, damping, and stiffness matrices, respectively and $\{Q_i\}$ is the element load vector for the ith element. The global matrices are obtained by the assembly of the element matrices. The global degree of freedom vector is denoted by $\{q\}$ and the global virtual displacement vector by $\{\delta q\}$. The global load vector $\{Q\}$ is formed by combining the element load vectors $\{Q_i\}$. The assembly of element inertia matrices $[M_i(q_i)]$ results in global inertia matrix $[M(q)]$

$$[M(q)] = \begin{bmatrix} \overleftarrow{N_s}\overrightarrow{N_s} & & & 0 \\ & [M_1] & [M_2] & \\ & & [M_3] & \ddots \\ 0 & & & [M_n] \end{bmatrix}$$

The matrix $[M]$ is a square matrix of order $5(n+1)$; it is also banded with the semibandwidth N_s equal to 10. The global damping and stiffness matrices $[C(q)]$ and $[K(q)]$ are obtained in the same manner. The matrix $[K]$ also is banded, whereas the matrix $[C]$ is nonbanded because of the presence of the double integral term

$$\int_0^{l_i}\int_0^{x} (\dot{v}'v' + \dot{w}'w')\,dx\,dx_i$$

in the expression for δT_i [Eq. (8)]. Matrix $[M]$ is symmetric, whereas matrices $[C]$ and $[K]$ are asymmetric. The substitution of Eq. (25) in Eq. (18) yields

$$\begin{aligned} \Delta = {} & \{\delta q\}^T[M(q)]\{\ddot{q}\} + \{\delta q\}^T[C(q)]\{\dot{q}\} \\ & + \{\delta q\}^T[K(q)]\{q\} - \{\delta q\}^T\{Q\} = 0 \end{aligned} \tag{26}$$

Since the virtual displacements $\{\delta q\}$ are arbitrary, Eq. (26) leads to the equations of motion

$$[M(q)]\{\ddot{q}\} + [C(q)]\{\dot{q}\} + [K(q)]\{q\} = \{Q\} \tag{27}$$

These equations are nonlinear in q. The bandedness of $[M]$ and $[K]$ helps reduce the storage space needed in computer programs since the zero elements off the band need not be stored.

Solution Procedure

Nonlinear Steady-State Solution

The first step in solving the equation of motion (27) is to get the steady trim solution. The steady-state equations are obtained by dropping all time dependent terms from Eq. (27)

$$[K_0(q_0)]\{q_0\} = \{Q_0\} \tag{28}$$

The steady-state stiffness matrix $[K_0]$ is asymmetric, banded, and a function of the steady displacement q_0; $\{Q_0\}$ is the steady-state load vector. The element matrices are evaluated numerically using Gauss quadrature formulas. The nonlinear Eq. (28) is solved iteratively using Brown's algorithm.[16] This finite-difference algorithm is a modified form of the Newton-Raphson method and the solution is obtained such that the sum of the squares of the errors in the equations is a minimum. The derivatives needed for this algorithm are evaluated numerically. The linear solution of Eq. (28) is used as the initial estimate in the solution procedure. The bandedness of $[K_0]$ is useful in two ways. The storage space needed in the computer program is less since only the elements within the band are stored. The number of computer operations is reduced considerably since the matrix operations corresponding to the zero entries of $[K_0]$, outside the band, are skipped.

For a given level of thrust, the pitch distribution θ of the blade is calculated from Eqs. (16), and then the corresponding

steady deflections are obtained. The torsional deflection changes the pitch of the blade. The new pitch at three-quarter span is $\theta_{0.75}+\phi_{0.75}$ and corresponding to this pitch value, a new thrust level is calculated. In general, the torsional stiffness of rotor blades is high, and the difference between the new and old values of thrust will be small.

Flutter Solution

After obtaining the steady-state solution, the next step is to get the flutter solution. For this purpose, the flutter motion is assumed to be a small perturbation ($\tilde{q}$) about the equilibrium position (q_0)

$$q=q_0+\tilde{q} \tag{29}$$

Substituting Eq. (29) into Eq. (27), subtracting Eq. (28), and keeping only linear perturbation terms, the flutter equations are obtained

$$[M(q_0)]\{\ddot{\tilde{q}}\}+[C(q_0)]\{\dot{\tilde{q}}\}+[K(q_0)]\{\tilde{q}\}=\{0\} \tag{30}$$

The normal mode method is used to obtain the eigenvalues of these equations and, hence, the natural modes are needed.

The coupled rotating natural modes of vibration about the equilibrium position are obtained by removing all aerodynamic terms and dropping the damping matrix from Eq. (30)

$$[M_s]\{\ddot{\tilde{q}}\}+[K_s]\{\tilde{q}\}=\{0\} \tag{31}$$

The mass and stiffness matrices $[M_s]$ and $[K_s]$ are symmetric and the eigenvalues (frequencies) of Eq. (31) are real. Again the bandedness of $[M_s]$ and $[K_s]$ is made use of effectively in the solution procedure.

The flutter equation of motion Eq. (30) is transformed to the modal space by writing

$$\{\tilde{q}\}=[\Phi]\{p\} \tag{32}$$

where $[\Phi]$ is the matrix of the first N eigenvectors (columnwise), and $\{p\}$ is the vector of N-generalized coordinates in the modal space. Substituting Eq. (32) into Eq. (30) and premultiplying by $[\Phi]^T$ yields the normal mode equation

$$[M^*]\{\ddot{p}\}+[C^*]\{\dot{p}\}+[K^*]\{p\}=\{0\} \tag{33}$$

Table 1 Values of parameters of uniform blade for numerical results

$EI_y/m\Omega^2R^4$	$=0.014486$ ($\omega_w=1.15$)	β_p	$=0.05$ rad
$EI_z/m\Omega^2R^4$	$=0.166908$ ($\omega_v=1.5$)	σ	$=0.1$
$GJ/m\Omega^2R^4$	$=0.000925$ ($\omega_\phi=2.5$)	γ	$=5$
	$=0.005661$ ($\omega_\phi=5$)		
k_{m1}/R	$=0$	a	$=6$
k_{m2}/R	$=0.025$	C_{D_0}	$=0.0095$
k_A/k_m	$=1.5$	$C_{M_{ac}}$	$=0$
c/R	$=\pi/40$	k_h	$=1.15$

Table 2 Steady tip deflections of a hingeless rotor blade ($C_T/\sigma=0.1$, $\beta_p=0.05$ rad, $\gamma=5.0$, $\omega_v=1.5$, $\omega_w=1.15$, $\omega_\phi=2.5$)

Number of elements	$v_{0_{tip}}$	$w_{0_{tip}}$	$\hat{\phi}_{0_{tip}}$
2	−0.00350	0.00487	−0.04386
3	−0.00342	0.00459	−0.04334
4	−0.00338	0.00446	−0.04315
5	−0.00337	0.00440	−0.04307
6	−0.00336	0.00436	−0.04302
7	−0.00335	0.00434	−0.04299
8	−0.00335	0.00433	−0.04297

The matrices $[M^*]$, $[C^*]$, and $[K^*]$ are nonsymmetric and are of order N. Equation (33) is solved as an algebraic eigenvalue problem, resulting in complex eigenvalues.

Boundary Conditions

Since the formulation of the problem is made using energy principles, the force boundary conditions, which are imbedded in the formulation, do not have to be considered separately. The nature of the displacement boundary conditions at the root determines the configuration of the rotor. For example, v, v', w, w', and $\hat{\phi}$ are zero at the root for a hingeless rotor blade; and for an articulated rotor blade, v, w, and $\hat{\phi}$ are zero at the hinge.

Results and Discussion

Numerical results are presented for two different rotor configurations, a hingeless rotor and an articulated rotor with a hinge offset of 6%. The chordwise offsets of the center of mass, the aerodynamic center, and torsion center from the elastic axis are considered to be zero. The section constants EB_1, EB_2, and the warping constants EC_1, EC_2, are taken to be zero. A precone (β_p) of 0.05 rad (2.9 deg), Lock number (γ) of 5, and solidity ratio (σ) of 0.1 are used.

Hingeless Rotor Blade

The blade properties selected for the stability analysis of a hingeless rotor blade are given in Table 1. The values for the

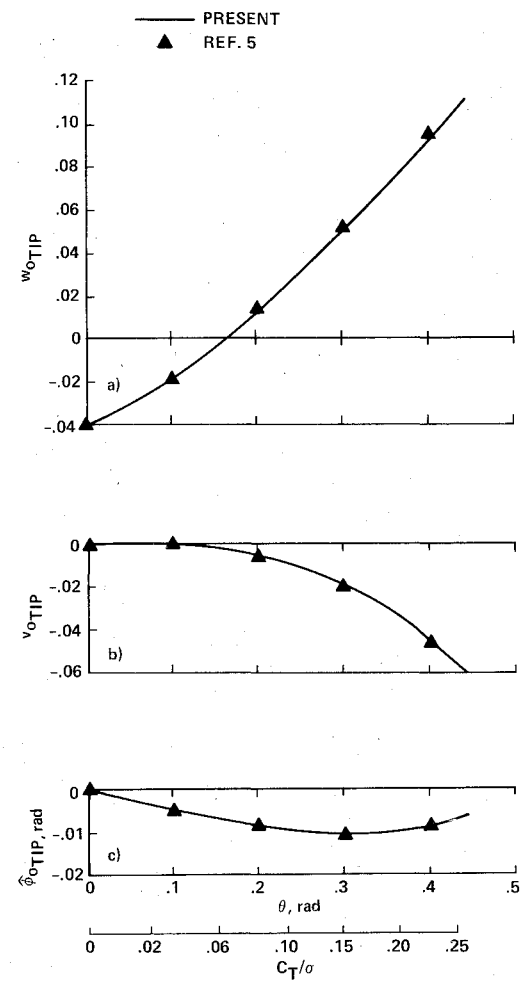

Fig. 4 a) Flap bending, b) lead-lag bending, and c) torsion. Steady tip deflections of a hingeless rotor blade; $\omega_v=1.5$, $\omega_w=1.15$, $\omega_\phi=5.0$, $\gamma=5.0$, $\beta_p=0.05$ rad.

Table 3 Fundamental coupled natural frequencies of a hingeless rotor blade
($C_T/\sigma = 0.1, \beta_p = 0.05$ rad, $\gamma = 5.0, \omega_v = 1.5, \omega_w = 1.15, \omega_\phi = 2.5$)

Number of elements	ω_v	ω_w	ω_ϕ
2	1.5196	1.1251	2.5105
3	1.5184	1.1221	2.4872
4	1.5182	1.1214	2.4787
5	1.5181	1.1212	2.4746
6	1.5181	1.1211	2.4724
7	1.5181	1.1211	2.4710
8	1.5180	1.1210	2.4702

Table 4 Real parts of the flutter eigenvalues of a hingeless rotor blade
($C_T/\sigma = 0.1, \beta_p = 0.05$ rad, $\gamma = 5.0, \omega_v = 1.5, \omega_w = 1.15, \omega_\phi = 2.5$)

Number of modes	Lag	Flap	Torsion
3	−0.03074	−0.31488	−0.35148
4	−0.03049	−0.31383	−0.35049
5	−0.03034	−0.31443	−0.35207
6	−0.03034	−0.31442	−0.35206
7	−0.03034	−0.31448	−0.35209

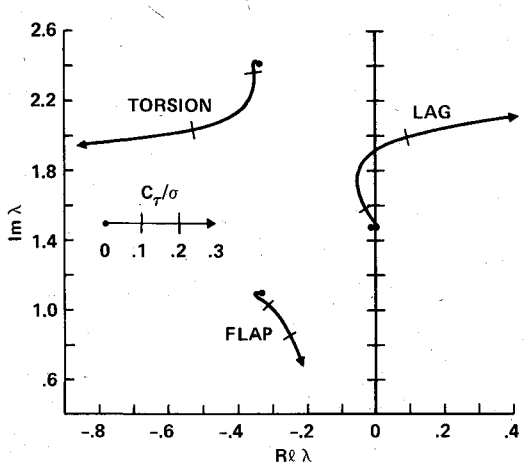

Fig. 5 Root locus plot for a hingeless rotor blade; $\omega_v = 1.5$, $\omega_w = 1.15$, $\omega_\phi = 2.5$, $\gamma = 5.0$, $\beta_p = 0.05$ rad.

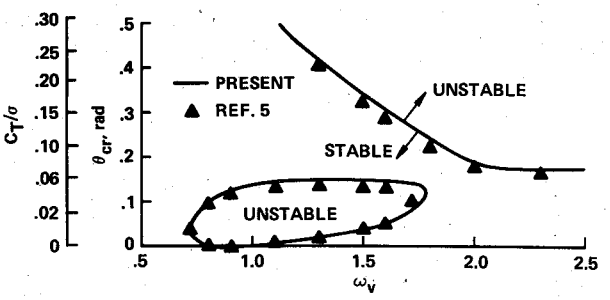

Fig. 6 Stability boundaries for a hingeless rotor blade; $\omega_w = 1.15$, $\omega_\phi = 2.5$, $\gamma = 5.0$, $\beta_p = 0.05$ rad.

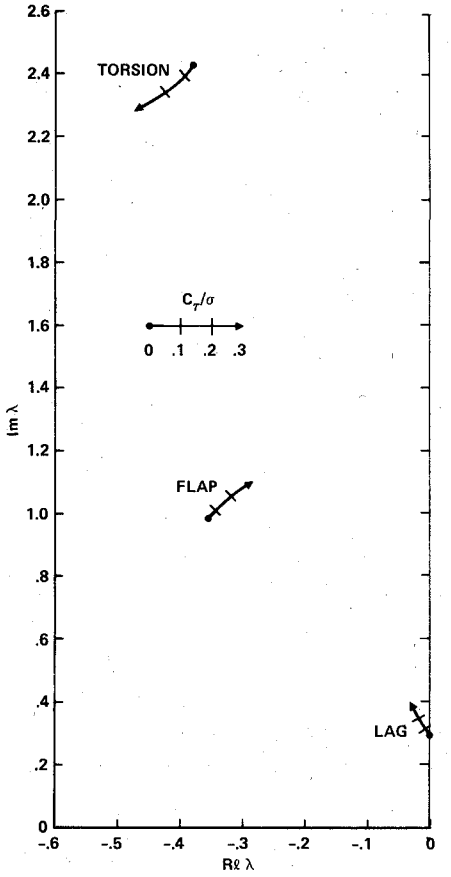

Fig. 7 Root locus plot for an articulated blade; hinge offset = 0.06, $\omega_\phi = 2.5$, $\gamma = 5.0$.

stiffness EI_y, EI_z, GJ, and the inertia parameters k_{m1}, k_{m2}, k_A are chosen such that the nondimensional rotating frequencies in the flap, lead-lag, and torsion directions are 1.15, 1.5, and 2.5, respectively. All blade properties are assumed to be uniform along the span of the blade.

The convergence of the steady-state deflections, using different numbers of finite elements is presented first. Table 2 shows the steady-state tip deflections $v_{0_{tip}}$, $w_{0_{tip}}$ (nondimensionalized with respect to the rotor length) and $\phi_{0_{tip}}$ (tip rotation in rad) as the total number of elements is varied from 2 to 8. The value of C_T/σ is 0.1. The results show, for the case considered, that six elements are sufficient for reasonably good convergence (three to four digit accuracy). The banded nature of the stiffness matrix reduces both the storage space and computation time required. For example, if eight elements are used, the full storage mode would require 2025 storage locations whereas the band storage mode needs only 855 locations for the stiffness matrix. Furthermore, the number of arithmetic operations involving the stiffness matrix is reduced by about 60%. The use of the linear solution makes the nonlinear iterative solution converge rapidly; only three or four iterations are needed for a converged solution. As a result, the computation time required for the nonlinear solution is small.

Figure 4 shows the steady tip deflections obtained using six elements for different levels of thrust C_T/σ (or θ). The fundamental torsional frequency is 5.0 for these results. The results of Hodges and Ormiston[5] are also shown in this figure. In Ref. 5, the steady deflections are obtained using the modal method with five nonrotating beam modes for each one of the deflections v_0, w_0, and ϕ_0. The agreement between the two results is good except at high thrust levels where a slight deviation appears. This may be due to the assumption in Ref. 5 that $\sin\theta \simeq \theta$ and $\cos\theta \simeq 1$ (not assumed here) for the calculation of aerodynamic loads, which may not be very accurate at high values of θ.

The rotating coupled natural frequencies of the blade about its steady deflected position are investigated for convergence as the number of finite elements is varied. Table 3 presents the fundamental lag, flap, and torsion frequencies with increasing number of elements. It is seen that six elements are sufficient

for four digit accuracy. Here, also, the bandedness of the inertia and stiffness matrices is used effectively to minimize computation time.

The solution of the flutter equations results in complex eigenvalues; the real and imaginary parts represent the damping and the frequency of the mode, respectively. The normal mode method is examined for convergence as the number of modes is varied, keeping the number of elements fixed at six. The real parts of the first three eigenvalues for different numbers of modes is given in Table 4. This table shows that five modes result in a well-converged solution (four digit accuracy). Figure 5 shows the root locus plot of the fundamental lead-lag, flap, and torsion modes as C_T/σ is varied from 0 to 0.3. Six finite elements and five normal modes are used in obtaining these results. The flap and torsion modes are stable over the entire range of C_T/σ considered, whereas the lead-lag mode is unstable for C_T/σ between 0.01 and 0.05 and above 0.17. The complete solution using six elements and five normal modes at a particular thrust level requires about 7 s of computation time on a CDC 7600 machine. Figure 6 shows the flutter stability boundaries as the lag frequency ω_v is varied. The results of Hodges and Ormiston[5] are also shown for comparison in this figure. In Ref. 5, the stability results are calculated using the normal mode method with five coupled rotating modes. There is general agreement between the two results. The differences that appear between the two results may be due to changes in aerodynamic forces by including all second-order terms (order ϵ^2) in the present analysis.

Articulated Rotor Blade

The same blade properties as given in Table 1 are used for the stability analysis of an articulated blade with a hinge offset of 6%. The convergence characteristics similar to the ones presented in Tables 2-4 were analyzed here also. The results confirmed the conclusions reached for the hingeless blade that about six elements and five normal modes are adequate for good accuracy (four digits). As before, only a few iterations result in a converged nonlinear trim solution. The flutter eigenvalues obtained using six finite elements and five coupled modes are shown in Fig. 7. All three modes are stable over the range of C_T/σ shown.

Conclusions

The finite element method has been applied successfully to determine the nonlinear trim deflections and the aeroelastic stability of flap-lag-torsion blades. The rotor blade is discretized into beam elements of ten degrees of freedom each. The equations of motion in terms of the nodal degrees of freedom are obtained using Hamilton's principle. Nonlinear steady deflections are obtained iteratively, solving the complete set of global equations, without making a modal transformation. The solution procedure is made efficient using the bandedness of the stiffness matrix, and the linear solution as the starting vector. The nonlinear solution converges in three or four iterations. The rotating natural modes of vibration are obtained about the steady deflected position of the blade. Numerical results have been presented for uniform hingeless and articulated rotor blades. Six finite elements are sufficient to determine the trim deflections and the free vibrations modes of a uniform blade. The linear flutter solution is obtained using the normal mode method; five coupled rotating modes are adequate to calculate the flutter eigenvalues of a uniform blade. The finite element application to rotor blade aeroelasticity has shown to be simple and efficient and thus has a great potential for treating complex blade geometries.

Appendix: Nondimensional Quantities

The nondimensional quantities in δU, δT, and δW [Eqs. (7-9)] are defined here. These symbols are retained after nondimensionalization.

Old quantity	New quantity	Assumed order of magnitude
x/R	x	1
$(\,')/\Omega$	$(\dot{})$	1
v/R	v	ϵ
w/R	w	ϵ
ϕ	ϕ	ϵ
θ	θ	1
$F/m_0\Omega^2R^2$	F	1
$EI_y/m_0\Omega^2R^4$	EI_y	1
$EI_z/m_0\Omega^2R^4$	EI_z	1
$GJ/m_0\Omega^2R^4$	GJ	1
$EA/m_0\Omega^2R^2$	EA	$1/\epsilon^2$
$EB_1/m_0\Omega^2R^6$	EB_1	ϵ^2
$EB_2/m_0\Omega^2R^5$	EB_2	ϵ
$EC_1/m_0\Omega^2R^6$	EC_1	ϵ^2
$EC_2/m_0\Omega^2R^5$	EC_2	ϵ
k_A/R	k_A	ϵ
k_{m1}/R	k_{m1}	ϵ
k_{m2}/R	k_{m2}	ϵ
e_a/R	e_a	$\epsilon^{3/2}$
e_g/R	e_g	$\epsilon^{3/2}$
β_p	β_p	ϵ

Acknowledgment

This research was sponsored by NASA Ames Research Center under NASA Grant NCC 2-13.

References

[1] Ormiston, R. A. and Hodges, D. H., "Linear Flap-Lag Dynamics of Hingeless Helicopter Rotor Blades in Hover," *Journal of the American Helicopter Society*, Vol. 17, April 1972, pp. 2-14.

[2] Houbolt, J. C. and Brooks, G. W., "Differential Equations of Motion for Combined Flapwise Bending, Chordwise Bending, and Torsion of Twisted, Nonuniform Rotor Blades," NACA Rept. 1346, 1958.

[3] Hodges, D. H. and Dowell, E. H., "Nonlinear Equations of Motion for Elastic Bending and Torsion of Twisted Nonuniform Blades," NASA TN D-7818, Dec. 1974.

[4] Hodges, D. H., Ormiston, R. A., and Peters, D. A., "On the Nonlinear Deformation Geometry of Euler-Bernoulli Beams," NASA TP 1566, April 1980.

[5] Hodges, D. H. and Ormiston, R. A., "Stability of Elastic Bending and Torsion of Uniform Cantilever Rotor Blades in Hover with Variable Structural Coupling," NASA TN D-8192, April 1976.

[6] Johnson, W., "Aeroelastic Analysis for Rotor-Craft in Flight or in a Wind Tunnel," NASA TN D-8515, July 1977.

[7] Gallagher, R. H., *Finite Element Analysis Fundamentals*, Prentice Hall, Inc., Englewood Cliffs, N.J., 1975.

[8] Nagaraj, V. T. and Shanthakumar, P., "Rotor Blade Vibrations by the Galerkin Finite Element Method," *Journal of Sound and Vibration*, Vol. 43, No. 3, 1975, pp. 575-577.

[9] Dzygadlo, Z. and Sobieraj, W., "Natural, Flexural-Torsional Vibration Analysis of Helicopter Rotor Blades by the Finite Element Method," *Journal of Technical Physics*, Vol. 18, No. 4, 1977, pp. 443-454.

[10] Hoa, S. V., "Vibration of a Rotating Beam with Tip Mass," *Journal of Sound and Vibration*, Vol. 67, No. 3, 1979, pp. 369-381.

[11] Hodges, D. H., "Vibration and Response of Nonuniform Rotating Beams with Discontinuities," *Journal of the American Helicopter Society*, Vol. 24, Oct. 1979, pp. 43-50.

[12] Murty, A.V.K. and Raman, A., "Non-Linear Dynamic Analysis of Rotors by Finite Element Method," *Journal of Sound and Vibration*, Vol. 69, No. 4, 1980, pp. 559-568.

[13] Yasue, M., "Gust Response and Alleviation for a Hingeless Helicopter Rotor in Cruising Flight," Ph.D. Dissertation, Dept. of Aeronautics, Massachusetts Institute of Technology, Sept. 1977.

[14] Friedmann, P. P. and Straub, F. K., "Application of the Finite Element Method to Rotary Wing Aeroelasticity," *Journal of the American Helicopter Society*, Vol. 25, Jan. 1980, pp. 36-44.

[15] Straub, F. K. and Friedmann, P. P., "A Galerkin Type Finite Element for Rotary-Wing Aeroelasticity in Hover and Forward Flight," *Vertica*, Vol. 5, 1981, pp. 75-98.

[16] Brown, K. M., "Computer Oriented Methods for Fitting Tabular Data in a Linear and Nonlinear Least Squares Sense," University of Minnesota, Dept. of Computer, Information, and Control Sciences, TR 72-13, 1972.